

UC Berkeley

UC Berkeley Previously Published Works

Title

Dalitz plot analyses of $B^0 \rightarrow D^- D^0 K^+$ and $B^+ \rightarrow D^- D^0 K^+$ decays

Permalink

<https://escholarship.org/uc/item/97t408dn>

Journal

Physical Review D, 91(5)

ISSN

2470-0010

Authors

Lees, JP
Poireau, V
Tisserand, V
[et al.](#)

Publication Date

2015-03-01

DOI

10.1103/physrevd.91.052002

Copyright Information

This work is made available under the terms of a Creative Commons Attribution License, available at <https://creativecommons.org/licenses/by/4.0/>

Peer reviewed

Dalitz plot analyses of $B^0 \rightarrow D^- D^0 K^+$ and $B^+ \rightarrow \bar{D}^0 D^0 K^+$ decays

J. P. Lees,¹ V. Poireau,¹ V. Tisserand,¹ E. Grauges,² A. Palano,^{3a,3b} G. Eigen,⁴ B. Stugu,⁴ D. N. Brown,⁵ L. T. Kerth,⁵ Yu. G. Kolomensky,⁵ M. J. Lee,⁵ G. Lynch,⁵ H. Koch,⁶ T. Schroeder,⁶ C. Hearty,⁷ T. S. Mattison,⁷ J. A. McKenna,⁷ R. Y. So,⁷ A. Khan,⁸ V. E. Blinov,^{9a,9b,9c} A. R. Buzykaev,^{9a} V. P. Druzhinin,^{9a,9b} V. B. Golubev,^{9a,9b} E. A. Kravchenko,^{9a,9b} A. P. Onuchin,^{9a,9b,9c} S. I. Serednyakov,^{9a,9b} Yu. I. Skovpen,^{9a,9b} E. P. Solodov,^{9a,9b} K. Yu. Todyshev,^{9a,9b} A. J. Lankford,¹⁰ B. Dey,¹¹ J. W. Gary,¹¹ O. Long,¹¹ C. Campagnari,¹² M. Franco Sevilla,¹² T. M. Hong,¹² D. Kovalskyi,¹² J. D. Richman,¹² C. A. West,¹² A. M. Eisner,¹³ W. S. Lockman,¹³ W. Panduro Vazquez,¹³ B. A. Schumm,¹³ A. Seiden,¹³ D. S. Chao,¹⁴ C. H. Cheng,¹⁴ B. Echenard,¹⁴ K. T. Flood,¹⁴ D. G. Hitlin,¹⁴ T. S. Miyashita,¹⁴ P. Ongmongkolkul,¹⁴ F. C. Porter,¹⁴ M. Röhrken,¹⁴ R. Andreassen,¹⁵ Z. Huard,¹⁵ B. T. Meadows,¹⁵ B. G. Pushpawela,¹⁵ M. D. Sokoloff,¹⁵ L. Sun,¹⁵ P. C. Bloom,¹⁶ W. T. Ford,¹⁶ A. Gaz,¹⁶ J. G. Smith,¹⁶ S. R. Wagner,¹⁶ R. Ayad,^{17,a} W. H. Toki,¹⁷ B. Spaan,¹⁸ D. Bernard,¹⁹ M. Verderi,¹⁹ S. Playfer,²⁰ D. Bettoni,^{21a} C. Bozzi,^{21a} R. Calabrese,^{21a,21b} G. Cibinetto,^{21a,21b} E. Fioravanti,^{21a,21b} I. Garzia,^{21a,21b} E. Luppi,^{21a,21b} L. Piemontese,^{21a} V. Santoro,^{21a} A. Calcaterra,²² R. de Sangro,²² G. Finocchiaro,²² S. Martellotti,²² P. Patteri,²² I. M. Peruzzi,^{22,b} M. Piccolo,²² M. Rama,²² A. Zallo,²² R. Contri,^{23a,23b} M. Lo Vetere,^{23a,23b} M. R. Monge,^{23a,23b} S. Passaggio,^{23a} C. Patrignani,^{23a,23b} E. Robutti,^{23a} B. Bhuyan,²⁴ V. Prasad,²⁴ A. Adametz,²⁵ U. Uwer,²⁵ H. M. Lacker,²⁶ U. Mallik,²⁷ C. Chen,²⁸ J. Cochran,²⁸ S. Prell,²⁸ H. Ahmed,²⁹ A. V. Gritsan,³⁰ N. Arnaud,³¹ M. Davier,³¹ D. Derkach,³¹ G. Grosdidier,³¹ F. Le Diberder,³¹ A. M. Lutz,³¹ B. Malaescu,^{31,c} P. Roudeau,³¹ A. Stocchi,³¹ G. Wormser,³¹ D. J. Lange,³² D. M. Wright,³² J. P. Coleman,³³ J. R. Fry,³³ E. Gabathuler,³³ D. E. Hutchcroft,³³ D. J. Payne,³³ C. Touramanis,³³ A. J. Bevan,³⁴ F. Di Lodovico,³⁴ R. Sacco,³⁴ G. Cowan,³⁵ D. N. Brown,³⁶ C. L. Davis,³⁶ A. G. Denig,³⁷ M. Fritsch,³⁷ W. Gradl,³⁷ K. Griessinger,³⁷ A. Hafner,³⁷ K. R. Schubert,³⁷ R. J. Barlow,^{38,d} G. D. Lafferty,³⁸ R. Cenci,³⁹ B. Hamilton,³⁹ A. Jawahery,³⁹ D. A. Roberts,³⁹ R. Cowan,⁴⁰ G. Sciolla,⁴⁰ R. Cheaib,⁴¹ P. M. Patel,^{41,e} S. H. Robertson,⁴¹ N. Neri,^{42a} F. Palombo,^{42a,42b} L. Cremaldi,⁴³ R. Godang,^{43,f} P. Sonnek,⁴³ D. J. Summers,⁴³ M. Simard,⁴⁴ P. Taras,⁴⁴ G. De Nardo,^{45a,45b} G. Onorato,^{45a,45b} C. Sciacca,^{45a,45b} M. Martinelli,⁴⁶ G. Raven,⁴⁶ C. P. Jessop,⁴⁷ J. M. LoSecco,⁴⁷ K. Honscheid,⁴⁸ R. Kass,⁴⁸ E. Feltresi,^{49a,49b} M. Margoni,^{49a,49b} M. Morandin,^{49a} M. Posocco,^{49a} M. Rotondo,^{49a} G. Simi,^{49a,49b} F. Simonetto,^{49a,49b} R. Stroili,^{49a,49b} S. Akar,⁵⁰ E. Ben-Haim,⁵⁰ M. Bomben,⁵⁰ G. R. Bonneaud,⁵⁰ H. Briand,⁵⁰ G. Calderini,⁵⁰ J. Chauveau,⁵⁰ Ph. Leruste,⁵⁰ G. Marchiori,⁵⁰ J. Ocariz,⁵⁰ M. Biasini,^{51a,51b} E. Manoni,^{51a} S. Pacetti,^{51a,51b} A. Rossi,^{51a} C. Angelini,^{52a,52b} G. Batignani,^{52a,52b} S. Bettarini,^{52a,52b} M. Carpinelli,^{52a,52b,g} G. Casarosa,^{52a,52b} A. Cervelli,^{52a,52b} M. Chrzaszcz,^{52a} F. Forti,^{52a,52b} M. A. Giorgi,^{52a,52b} A. Lusiani,^{52a,52c} B. Oberhof,^{52a,52b} E. Paoloni,^{52a,52b} A. Perez,^{52a} G. Rizzo,^{52a,52b} J. J. Walsh,^{52a} D. Lopes Pegna,⁵³ J. Olsen,⁵³ A. J. S. Smith,⁵³ F. Anulli,^{54a} R. Faccini,^{54a,54b} F. Ferrarotto,^{54a} F. Ferroni,^{54a,54b} M. Gaspero,^{54a,54b} L. Li Gioi,^{54a} A. Pilloni,^{54a,54b} G. Piredda,^{54a} C. Büniger,⁵⁵ S. Dittrich,⁵⁵ O. Grünberg,⁵⁵ M. Hess,⁵⁵ T. Leddig,⁵⁵ C. Voß,⁵⁵ R. Waldi,⁵⁵ T. Adye,⁵⁶ E. O. Olaiya,⁵⁶ F. F. Wilson,⁵⁶ S. Emery,⁵⁷ G. Vasseur,⁵⁷ D. Aston,⁵⁸ D. J. Bard,⁵⁸ C. Cartaro,⁵⁸ M. R. Convery,⁵⁸ J. Dorfan,⁵⁸ G. P. Dubois-Felsmann,⁵⁸ W. Dunwoodie,⁵⁸ M. Ebert,⁵⁸ R. C. Field,⁵⁸ B. G. Fulsom,⁵⁸ M. T. Graham,⁵⁸ C. Hast,⁵⁸ W. R. Innes,⁵⁸ P. Kim,⁵⁸ D. W. G. S. Leith,⁵⁸ D. Lindemann,⁵⁸ S. Luitz,⁵⁸ V. Luth,⁵⁸ H. L. Lynch,⁵⁸ D. B. MacFarlane,⁵⁸ D. R. Muller,⁵⁸ H. Neal,⁵⁸ M. Perl,^{58,e} T. Pulliam,⁵⁸ B. N. Ratcliff,⁵⁸ A. Roodman,⁵⁸ A. A. Salnikov,⁵⁸ R. H. Schindler,⁵⁸ A. Snyder,⁵⁸ D. Su,⁵⁸ M. K. Sullivan,⁵⁸ J. Va'vra,⁵⁸ W. J. Wisniewski,⁵⁸ H. W. Wulsin,⁵⁸ M. V. Purohit,⁵⁹ R. M. White,^{59,h} J. R. Wilson,⁵⁹ A. Randle-Conde,⁶⁰ S. J. Sekula,⁶⁰ M. Bellis,⁶¹ P. R. Burchat,⁶¹ E. M. T. Puccio,⁶¹ M. S. Alam,⁶² J. A. Ernst,⁶² R. Gorodeisky,⁶³ N. Guttman,⁶³ D. R. Peimer,⁶³ A. Soffer,⁶³ S. M. Spanier,⁶⁴ J. L. Ritchie,⁶⁵ R. F. Schwitters,⁶⁵ B. C. Wray,⁶⁵ J. M. Izen,⁶⁶ X. C. Lou,⁶⁶ F. Bianchi,^{67a,67b} F. De Mori,^{67a,67b} A. Filippi,^{67a} D. Gamba,^{67a,67b} L. Lanceri,^{68a,68b} L. Vitale,^{68a,68b} F. Martinez-Vidal,⁶⁹ A. Oyanguren,⁶⁹ P. Villanueva-Perez,⁶⁹ J. Albert,⁷⁰ Sw. Banerjee,⁷⁰ A. Beaulieu,⁷⁰ F. U. Bernlochner,⁷⁰ H. H. F. Choi,⁷⁰ G. J. King,⁷⁰ R. Kowalewski,⁷⁰ M. J. Lewczuk,⁷⁰ T. Lueck,⁷⁰ I. M. Nugent,⁷⁰ J. M. Roney,⁷⁰ R. J. Sobie,⁷⁰ N. Tasneem,⁷⁰ T. J. Gershon,⁷¹ P. F. Harrison,⁷¹ T. E. Latham,⁷¹ H. R. Band,⁷² S. Dasu,⁷² Y. Pan,⁷² R. Prepost,⁷² and S. L. Wu⁷²

(BABAR Collaboration)

¹Laboratoire d'Annecy-le-Vieux de Physique des Particules (LAPP), Université de Savoie, CNRS/IN2P3, F-74941 Annecy-Le-Vieux, France²Universitat de Barcelona, Facultat de Física, Departament ECM, E-08028 Barcelona, Spain^{3a}INFN Sezione di Bari, I-70126 Bari, Italy^{3b}Dipartimento di Fisica, Università di Bari, I-70126 Bari, Italy⁴University of Bergen, Institute of Physics, N-5007 Bergen, Norway⁵Lawrence Berkeley National Laboratory and University of California, Berkeley, California 94720, USA⁶Ruhr Universität Bochum, Institut für Experimentalphysik 1, D-44780 Bochum, Germany⁷University of British Columbia, Vancouver, British Columbia, Canada V6T 1Z1⁸Brunel University, Uxbridge, Middlesex UB8 3PH, United Kingdom^{9a}Budker Institute of Nuclear Physics SB RAS, Novosibirsk 630090, Russia

- ^{9b}*Novosibirsk State University, Novosibirsk 630090, Russia*
- ^{9c}*Novosibirsk State Technical University, Novosibirsk 630092, Russia*
- ¹⁰*University of California at Irvine, Irvine, California 92697, USA*
- ¹¹*University of California at Riverside, Riverside, California 92521, USA*
- ¹²*University of California at Santa Barbara, Santa Barbara, California 93106, USA*
- ¹³*University of California at Santa Cruz, Institute for Particle Physics, Santa Cruz, California 95064, USA*
- ¹⁴*California Institute of Technology, Pasadena, California 91125, USA*
- ¹⁵*University of Cincinnati, Cincinnati, Ohio 45221, USA*
- ¹⁶*University of Colorado, Boulder, Colorado 80309, USA*
- ¹⁷*Colorado State University, Fort Collins, Colorado 80523, USA*
- ¹⁸*Technische Universität Dortmund, Fakultät Physik, D-44221 Dortmund, Germany*
- ¹⁹*Laboratoire Leprince-Ringuet, Ecole Polytechnique, CNRS/IN2P3, F-91128 Palaiseau, France*
- ²⁰*University of Edinburgh, Edinburgh EH9 3JZ, United Kingdom*
- ^{21a}*INFN Sezione di Ferrara, I-44122 Ferrara, Italy*
- ^{21b}*Dipartimento di Fisica e Scienze della Terra, Università di Ferrara, I-44122 Ferrara, Italy*
- ²²*INFN Laboratori Nazionali di Frascati, I-00044 Frascati, Italy*
- ^{23a}*INFN Sezione di Genova, I-16146 Genova, Italy*
- ^{23b}*Dipartimento di Fisica, Università di Genova, I-16146 Genova, Italy*
- ²⁴*Indian Institute of Technology Guwahati, Guwahati, Assam 781 039, India*
- ²⁵*Universität Heidelberg, Physikalisches Institut, D-69120 Heidelberg, Germany*
- ²⁶*Humboldt-Universität zu Berlin, Institut für Physik, D-12489 Berlin, Germany*
- ²⁷*University of Iowa, Iowa City, Iowa 52242, USA*
- ²⁸*Iowa State University, Ames, Iowa 50011-3160, USA*
- ²⁹*Physics Department, Jazan University, Jazan 22822, Kingdom of Saudi Arabia*
- ³⁰*Johns Hopkins University, Baltimore, Maryland 21218, USA*
- ³¹*Laboratoire de l'Accélérateur Linéaire, IN2P3/CNRS et Université Paris-Sud 11, Centre Scientifique d'Orsay, F-91898 Orsay Cedex, France*
- ³²*Lawrence Livermore National Laboratory, Livermore, California 94550, USA*
- ³³*University of Liverpool, Liverpool L69 7ZE, United Kingdom*
- ³⁴*Queen Mary, University of London, London E1 4NS, United Kingdom*
- ³⁵*University of London, Royal Holloway and Bedford New College, Egham, Surrey TW20 0EX, United Kingdom*
- ³⁶*University of Louisville, Louisville, Kentucky 40292, USA*
- ³⁷*Johannes Gutenberg-Universität Mainz, Institut für Kernphysik, D-55099 Mainz, Germany*
- ³⁸*University of Manchester, Manchester M13 9PL, United Kingdom*
- ³⁹*University of Maryland, College Park, Maryland 20742, USA*
- ⁴⁰*Massachusetts Institute of Technology, Laboratory for Nuclear Science, Cambridge, Massachusetts 02139, USA*
- ⁴¹*McGill University, Montréal, Québec, Canada H3A 2T8*
- ^{42a}*INFN Sezione di Milano, I-20133 Milano, Italy*
- ^{42b}*Dipartimento di Fisica, Università di Milano, I-20133 Milano, Italy*
- ⁴³*University of Mississippi, University, Mississippi 38677, USA*
- ⁴⁴*Université de Montréal, Physique des Particules, Montréal, Québec, Canada H3C 3J7*
- ^{45a}*INFN Sezione di Napoli, I-80126 Napoli, Italy*
- ^{45b}*Dipartimento di Scienze Fisiche, Università di Napoli Federico II, I-80126 Napoli, Italy*
- ⁴⁶*NIKHEF, National Institute for Nuclear Physics and High Energy Physics, NL-1009 DB Amsterdam, The Netherlands*
- ⁴⁷*University of Notre Dame, Notre Dame, Indiana 46556, USA*
- ⁴⁸*Ohio State University, Columbus, Ohio 43210, USA*
- ^{49a}*INFN Sezione di Padova, I-35131 Padova, Italy*
- ^{49b}*Dipartimento di Fisica, Università di Padova, I-35131 Padova, Italy*
- ⁵⁰*Laboratoire de Physique Nucléaire et de Hautes Energies, IN2P3/CNRS, Université Pierre et Marie Curie-Paris6, Université Denis Diderot-Paris7, F-75252 Paris, France*
- ^{51a}*INFN Sezione di Perugia, I-06123 Perugia, Italy*
- ^{51b}*Dipartimento di Fisica, Università di Perugia, I-06123 Perugia, Italy*
- ^{52a}*INFN Sezione di Pisa, I-56127 Pisa, Italy*
- ^{52b}*Dipartimento di Fisica, Università di Pisa, I-56127 Pisa, Italy*
- ^{52c}*Scuola Normale Superiore di Pisa, I-56127 Pisa, Italy*
- ⁵³*Princeton University, Princeton, New Jersey 08544, USA*
- ^{54a}*INFN Sezione di Roma, I-00185 Roma, Italy*

- ^{54b}*Dipartimento di Fisica, Università di Roma La Sapienza, I-00185 Roma, Italy*
⁵⁵*Universität Rostock, D-18051 Rostock, Germany*
⁵⁶*Rutherford Appleton Laboratory, Chilton, Didcot, Oxon OX11 0QX, United Kingdom*
⁵⁷*CEA, Irfu, SPP, Centre de Saclay, F-91191 Gif-sur-Yvette, France*
⁵⁸*SLAC National Accelerator Laboratory, Stanford, California 94309, USA*
⁵⁹*University of South Carolina, Columbia, South Carolina 29208, USA*
⁶⁰*Southern Methodist University, Dallas, Texas 75275, USA*
⁶¹*Stanford University, Stanford, California 94305-4060, USA*
⁶²*State University of New York, Albany, New York 12222, USA*
⁶³*Tel Aviv University, School of Physics and Astronomy, Tel Aviv 69978, Israel*
⁶⁴*University of Tennessee, Knoxville, Tennessee 37996, USA*
⁶⁵*University of Texas at Austin, Austin, Texas 78712, USA*
⁶⁶*University of Texas at Dallas, Richardson, Texas 75083, USA*
^{67a}*INFN Sezione di Torino, I-10125 Torino, Italy*
^{67b}*Dipartimento di Fisica, Università di Torino, I-10125 Torino, Italy*
^{68a}*INFN Sezione di Trieste, I-34127 Trieste, Italy*
^{68b}*Dipartimento di Fisica, Università di Trieste, I-34127 Trieste, Italy*
⁶⁹*IFIC, Universitat de Valencia-CSIC, E-46071 Valencia, Spain*
⁷⁰*University of Victoria, Victoria, British Columbia, Canada V8W 3P6*
⁷¹*Department of Physics, University of Warwick, Coventry CV4 7AL, United Kingdom*
⁷²*University of Wisconsin, Madison, Wisconsin 53706, USA*
(Received 23 December 2014; published 2 March 2015)

We present Dalitz plot analyses for the decays of B mesons to $D^-D^0K^+$ and $\bar{D}^0D^0K^+$. We report the observation of the $D_{s1}^*(2700)^+$ resonance in these two channels and obtain measurements of the mass $M(D_{s1}^*(2700)^+) = 2699_{-7}^{+14}$ MeV/ c^2 and of the width $\Gamma(D_{s1}^*(2700)^+) = 127_{-19}^{+24}$ MeV, including statistical and systematic uncertainties. In addition, we observe an enhancement in the D^0K^+ invariant mass around 2350–2500 MeV/ c^2 in both decays $B^0 \rightarrow D^-D^0K^+$ and $B^+ \rightarrow \bar{D}^0D^0K^+$, which we are not able to interpret. The results are based on 429 fb $^{-1}$ of data containing $471 \times 10^6 B\bar{B}$ pairs collected at the $\Upsilon(4S)$ resonance with the *BABAR* detector at the SLAC National Accelerator Laboratory.

DOI: 10.1103/PhysRevD.91.052002

PACS numbers: 13.25.Hw, 14.40.Nd

I. INTRODUCTION

In the $B \rightarrow \bar{D}^{(*)}D^{(*)}K$ final states [1], where D is a D^0 or a D^+ , D^* is a D^{*0} or D^{*+} , and K is a K^+ or a K^0 , we have the possibility to search for $\bar{D}^{(*)}D^{(*)}$ resonances (charmonium or charmoniumlike resonances) as well as $D^{(*)}K$ resonances ($c\bar{s}$ resonances). These final states have been useful in the past to determine properties of the $D_{s1}(2536)$ and $\psi(3770)$ mesons and of the $X(3872)$ state at *BABAR* [2] and Belle [3,4] as well as the $D_{s1}^*(2700)^+$ meson at Belle [4]. These analyses, based on the studies of invariant

mass distributions, were able to extract properties such as the mass, width, and spin of the resonances.

The analysis presented here gives useful information about $c\bar{s}$ mesons present in these decays. Before 2003 only four $c\bar{s}$ mesons were known and their properties were consistent with the predictions of potential models [5]. Since then the $D_{s0}^*(2317)$ and $D_{s1}(2460)$ states have been discovered by *BABAR* and CLEO [6] with widths and masses in disagreement with the expectations. The $D_{s1}^*(2700)^+$ meson was discovered by *BABAR* decaying to DK in inclusive e^+e^- interactions [7] and confirmed by Belle in the final state $B^+ \rightarrow \bar{D}^0D^0K^+$ [4]. The LHCb experiment studied the $D_{s1}^*(2700)^+$ meson in the $D^+K_S^0$ and D^0K^+ final states [8] and obtained a more precise determination of its properties. The $D_{s1}^*(2700)^+$ meson was also observed in inclusive e^+e^- interactions decaying to D^*K [7]. An additional $c\bar{s}$ state, the $D_{sJ}^*(2860)^+$, was discovered by *BABAR* decaying to DK and D^*K [7] and confirmed by LHCb [8]. Recently, LHCb claimed that the structure at 2.86 GeV/ c^2 was an admixture of spin-1 and spin-3 resonances [9]. Finally, the $D_{sJ}(3040)^+$ meson was observed in the D^*K final state by *BABAR* [7].

In this study, we perform Dalitz plot analyses for the channels $B^0 \rightarrow D^-D^0K^+$ and $B^+ \rightarrow \bar{D}^0D^0K^+$ which

^aPresent address: University of Tabuk, Tabuk 71491, Saudi Arabia.

^bAlso at Università di Perugia, Dipartimento di Fisica, I-06123 Perugia, Italy.

^cPresent address: Laboratoire de Physique Nucléaire et de Hautes Energies, IN2P3/CNRS, F-75252 Paris, France.

^dPresent address: University of Huddersfield, Huddersfield HD1 3DH, United Kingdom.

^eDeceased.

^fPresent address: University of South Alabama, Mobile, Alabama 36688, USA.

^gAlso at Università di Sassari, I-07100 Sassari, Italy.

^hPresent address: Universidad Técnica Federico Santa María, 2390123 Valparaíso, Chile.

contain only pseudoscalar particles in the three-body decay. These Dalitz plot analyses allow the interferences between the different amplitudes which are present in the final states to be taken into account correctly. This is the first time that such Dalitz plot analyses have been performed for these decays.

II. THE BABAR DETECTOR AND DATA SAMPLE

The data were recorded by the *BABAR* detector at the PEP-II asymmetric-energy e^+e^- storage ring operating at the SLAC National Accelerator Laboratory. We analyze the complete *BABAR* data sample collected at the $\Upsilon(4S)$ resonance corresponding to an integrated luminosity of 429 fb^{-1} [10], giving $N_{B\bar{B}} = (470.9 \pm 0.1 \pm 2.8) \times 10^6$ $B\bar{B}$ pairs produced, where the first uncertainty is statistical and the second systematic.

The *BABAR* detector is described in detail elsewhere [11]. Charged particles are detected and their momenta measured with a five-layer silicon vertex tracker and a 40-layer drift chamber in a 1.5 T axial magnetic field. Charged particle identification is based on the measurements of the energy loss in the tracking devices and of the Cherenkov radiation in the ring-imaging detector. The energies and locations of showers associated with photons are measured in the electromagnetic calorimeter. Muons are identified by the instrumented magnetic-flux return, which is located outside the magnet.

We employ a Monte Carlo simulation to study the relevant backgrounds and estimate the selection efficiencies. We use EVTGEN [12] to model the kinematics of B mesons and JETSET [13] to model continuum processes, $e^+e^- \rightarrow q\bar{q}$ ($q = u, d, s, c$). The *BABAR* detector and its response to particle interactions are modeled using the GEANT4 [14] simulation package.

III. EVENT SELECTION AND SIGNAL YIELDS

The selection and reconstruction of $B^0 \rightarrow D^-D^0K^+$ and $B^+ \rightarrow \bar{D}^0D^0K^+$, along with 20 other $B \rightarrow \bar{D}^{(*)}D^{(*)}K$ modes, is described in Ref. [15]. We briefly summarize the selection criteria in this section. We reconstruct D mesons in the modes $D^0 \rightarrow K^-\pi^+$, $K^-\pi^+\pi^0$, $K^-\pi^+\pi^-\pi^+$, and $D^+ \rightarrow K^-\pi^+\pi^+$. The B candidates are reconstructed by combining a \bar{D} (representing either a D^- or a \bar{D}^0), a D^0 , and a K^+ candidate. For the mode $B^+ \rightarrow \bar{D}^0D^0K^+$, at least one of the D^0 mesons is required to decay to $K^-\pi^+$. A mass-constrained kinematic fit is applied to the intermediate particles (D^0 , D^+ , π^0) to improve their momentum resolution and the resolution of the invariant masses of the studied resonances.

Two kinematic variables are used to isolate the B -meson signal. The first variable is the beam-energy-substituted mass defined as

$$m_{\text{ES}} = \sqrt{\left(\frac{s/2 + \vec{p}_0 \cdot \vec{p}_B}{E_0}\right)^2 - |\vec{p}_B|^2}, \quad (1)$$

where \sqrt{s} is the e^+e^- center-of-mass energy. For the momenta in the laboratory frame, \vec{p}_0 , \vec{p}_B , and the energy, E_0 , the subscripts 0 and B refer to the e^+e^- system and the reconstructed B meson, respectively. The other variable is ΔE , the difference between the reconstructed energy of the B candidate and the beam energy in the e^+e^- center-of-mass frame. Signal events have m_{ES} compatible with the known B -meson mass [16] and ΔE compatible with 0 MeV, within their respective resolutions.

For the modes $B^0 \rightarrow D^-D^0K^+$ and $B^+ \rightarrow \bar{D}^0D^0K^+$, we obtain 1.1 and 1.3 B candidates per event on average, respectively. If more than one candidate is selected in an event, we retain only the one with the smallest value of $|\Delta E|$. According to Monte Carlo studies, this criterion finds the correct candidate, when present in the candidate list, in more than 95% of the cases for the two final states. We keep only events with $|\Delta E| < 10\text{--}14$ MeV depending on the D final state [15].

In order to obtain the signal and background yields, fits are performed on the m_{ES} distributions, as described in detail in Ref. [15]. The probability density function (PDF) of the signal is determined from Monte Carlo samples. A Crystal Ball function [17] (Gaussian PDF modified to include a power-law tail on the low side of the peak) is used to describe the signal. The background contribution is the sum of cross-feed events and combinatorial background. The cross-feed background to a mode consists of all incorrectly reconstructed $B \rightarrow \bar{D}^{(*)}D^{(*)}K$ events. The ratio of cross-feed events to signal events is 11% for $B^0 \rightarrow D^-D^0K^+$ and 17% for $B^+ \rightarrow \bar{D}^0D^0K^+$. The cross-feed events are described by the sum of an ARGUS function [18] and a Gaussian function, where the latter allows us to take into account the cross-feed events peaking in the signal region. For both modes, the Gaussian part represents a negligible contribution to the total cross feed. Since the fit for the yield for one channel uses as input the branching fractions from other channels, an iterative procedure using the 22 $B \rightarrow \bar{D}^{(*)}D^{(*)}K$ modes is employed [15]. The combinatorial background events are described by the sum of an ARGUS function and a Gaussian function, reflecting the fact that a small fraction of events peaks in the signal region (coming for example from $\bar{D}D^0K^+$ events where one of the D mesons is not decaying to a studied mode). The fits performed on the m_{ES} distributions using the sum of the PDFs for the signal and for the background are shown in Fig. 1. We obtain 635 ± 47 and 901 ± 54 signal events for $B^0 \rightarrow D^-D^0K^+$ and $B^+ \rightarrow \bar{D}^0D^0K^+$, respectively [15].

We impose an additional condition to enhance the purity for the Dalitz plot analysis. We require $5.275 < m_{\text{ES}} < 5.284 \text{ GeV}/c^2$, obtaining a total number of 1470 events with a signal purity of $(38.6 \pm 2.8 \pm 2.1)\%$ for

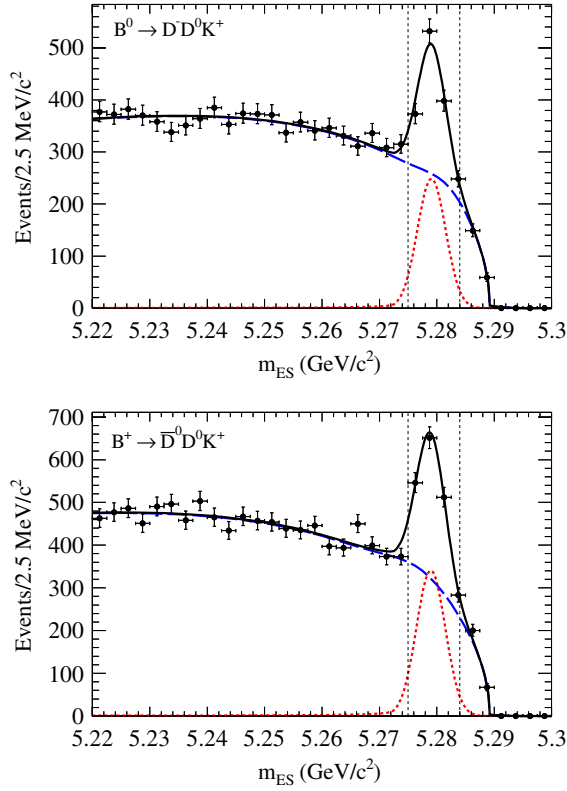


FIG. 1 (color online). Fits of the m_{ES} data distributions [15] for the modes $B^0 \rightarrow D^- D^0 K^+$ (top) and $B^+ \rightarrow \bar{D}^0 D^0 K^+$ (bottom). Points with statistical errors are data events, the red dashed line represents the signal PDF, the blue dashed line represents the background PDF, and the black solid line shows the total PDF. The vertical lines indicate the signal region used in the rest of the analysis.

$B^0 \rightarrow D^- D^0 K^+$ and obtaining a total of 1894 events with a signal purity of $(41.6 \pm 2.5 \pm 3.1)\%$ for $B^+ \rightarrow \bar{D}^0 D^0 K^+$, where the first uncertainties are statistical and the second systematic.

IV. DALITZ PLOT ANALYSES

A. Method

We use an isobar model formalism to perform the Dalitz plot analysis [19]. The decays are described by a sum of amplitudes representing nonresonant and resonant contributions:

$$\mathcal{M} = \sum_i c_i A_i, \quad (2)$$

where the $c_i \equiv \rho_i e^{i\phi_i}$ are complex coefficients of modulus $\rho_i \equiv |c_i|$ and phase ϕ_i . The quantities A_i are complex amplitudes and can be written as

$$A_i = D_i \times T_i(\Omega), \quad (3)$$

where D_i represents the dynamical function describing the i th intermediate resonance, and $T_i(\Omega)$ represents the angular distribution of the final state particles as a function of the solid angle Ω . For nonresonant events, we have $A_i = 1$. The quantity D_i is parametrized by a Breit-Wigner function, whose expression for a resonance $r \rightarrow AB$ is given by

$$D = \frac{F_B F_r}{M_r^2 - M_{AB}^2 - i\Gamma_{AB} M_r}, \quad (4)$$

where F_B and F_r are the Blatt-Weisskopf damping factors for the B meson and for the resonance, M_r is the mass of the resonance, M_{AB} the invariant mass of the system AB , and Γ_{AB} its mass-dependent width. The expression for the mass-dependent width is

$$\Gamma_{AB} = \Gamma_r \left(\frac{p_{AB}}{p_r} \right)^{2J+1} \left(\frac{M_r}{M_{AB}} \right) F_r^2, \quad (5)$$

where Γ_r and J are the width and the spin of the resonance. The quantity p_{AB} is the momentum of either daughter in the AB rest frame, and p_r is the value of p_{AB} when $M_{AB} = M_r$. The resonances we study here have a large enough natural width and we can ignore the effect of the detector resolutions.

The exact expressions of the Blatt-Weisskopf factors [20] are given in Ref. [21] and depend on the momenta of the particles involved, on the spin of the resonance, and on the radius of the Blatt-Weisskopf barrier. For the B meson and for the intermediate resonance, we use a radius of 1.5 GeV^{-1} . The angular term $T_i(\Omega)$ is also given in Ref. [21] and depends on the masses of the particles involved in the reaction as well as on the spin of the intermediate resonance.

We extract the complex amplitudes present in the data (from their modulus ρ_i and phase ϕ_i) and the mass and width of the $D_{s1}^*(2700)^+$ resonance. To obtain these parameters, we perform an unbinned maximum likelihood fit where the likelihood function for the event n can be written as

$$\mathcal{L}_n = p \times \varepsilon_i(m_1^2, m_2^2) \times \frac{|\mathcal{M}|^2}{\int |\mathcal{M}|^2 \varepsilon(m_1^2, m_2^2) dm_1^2 dm_2^2} + (1-p) \times \frac{B(m_1^2, m_2^2)}{\int B(m_1^2, m_2^2) dm_1^2 dm_2^2}, \quad (6)$$

where $|\mathcal{M}|^2 = \sum_{i,j} c_i c_j^* A_i A_j^*$ is calculated for the event n . In this expression, m_1 and m_2 represent the invariant mass of $\bar{D}D^0$ and $D^0 K^+$ for the event n . The quantity p corresponds to the purity of the signal. The function $\varepsilon(m_1^2, m_2^2)$ is the efficiency across the Dalitz plot, and the function $B(m_1^2, m_2^2)$ represents the background in the Dalitz plot. The integrals are computed using Monte Carlo events: since we use varying resonance parameters, the

integration is performed at each minimization step. We minimize the total negative log likelihood,

$$\mathcal{F} = \sum_n -2 \times \log(\mathcal{L}_n), \quad (7)$$

where the index n represents a particular event and the sum is performed over the total number of events. We compare the different fits using $\Delta\mathcal{F} = \mathcal{F} - \mathcal{F}_{\text{nominal}}$, where \mathcal{F} is the value of the total negative log likelihood for a given fit and $\mathcal{F}_{\text{nominal}}$ is this value for the nominal fit defined below. We are sensitive only to relative moduli and phases, which means we are free to fix one modulus and one phase. We choose the $D_{s1}^*(2700)^+$ resonance as the reference amplitude with assignments $|c_{D_{s1}^*(2700)^+}| = 1$ and $\phi_{D_{s1}^*(2700)^+} = 0$.

A Monte Carlo simulation is performed using the fit results and is superimposed on the data in the Dalitz plot or on invariant mass projections. In addition to the value of \mathcal{F} , we compute the quantity χ^2/n_{dof} , where n_{dof} is the number of degrees of freedom, computed as the number of bins in the Dalitz plot minus the number of free parameters in the fit. We use an adaptive size for the bins so that each bin contains at least 15 events to get an approximately Gaussian behavior.

The fit fraction for each amplitude is defined as

$$f_i = \frac{|c_i|^2 \int |A_i|^2 dm_1^2 dm_2^2}{\sum_{j,k} c_j c_k^* \int A_j A_k^* dm_1^2 dm_2^2}. \quad (8)$$

The fit fractions do not necessarily add up to 1, due to the interferences that can take place between the different final states. The errors on the fit fractions are evaluated by propagating the full covariance matrix obtained from the fit.

The initial values of the parameters are randomized inside their bounds and 250 different fits are performed with these randomized initial values. We choose the fit which presents the smallest value of the total negative log likelihood \mathcal{F} , which allows us to avoid local minima and to obtain the global minimum of the negative log likelihood.

B. Efficiency and background determination

As seen in Eq. (6), the efficiency variation over the Dalitz plot needs to be parametrized. We employ Monte Carlo simulations of the signal events for each reconstructed D decay for the modes $B^0 \rightarrow D^- D^0 K^+$ and $B^+ \rightarrow \bar{D}^0 D^0 K^+$. The signal density is simulated as being constant over the Dalitz plot. We divide the Dalitz plot in bins of size 0.36×0.53 (GeV^2/c^4)². For each two-dimensional bin, we divide the number of simulated signal events after selection and reconstruction by the generated number of events. We combine neighboring bins with low statistics so that each bin has more than ten simulated events after the reconstruction. We obtain a mapping of the efficiency for each reconstructed D mode and combine these mappings

by weighting them together according to the D secondary branching fractions.

To obtain the function $\epsilon(m_1^2, m_2^2)$ of Eq. (6), we use a bilinear two-dimensional interpolation method applied on the global efficiency mapping. The interpolation makes use of the four values from the bins around a given mass coordinate to compute the efficiency. At the edge of the mapping, we use the value of the bin without interpolation to avoid bias toward a null efficiency.

The background distribution in the Dalitz plot is described by the function $B(m_1^2, m_2^2)$ of Eq. (6). We observe that the Monte Carlo simulation reproduces correctly the data by comparing events in the m_{ES} sideband ($m_{\text{ES}} < 5.26$ GeV/c^2) between the data and the simulation. We therefore employ a Monte Carlo simulation of background events, using the same reconstruction and selection as in the data. We obtain a distribution of the background in the Dalitz plot using bins of size 0.27×0.37 (GeV^2/c^4)². The distribution of the background includes the contribution from the combinatorial background (including the background which peaks in the signal region), and we check that the small proportion of cross-feed events has a similar distribution as the background in the Dalitz plot. The background distribution is interpolated with a bilinear two-dimensional method to get the value at any coordinate.

C. Fits of the Dalitz plots

The Dalitz plots for $B^0 \rightarrow D^- D^0 K^+$ and $B^+ \rightarrow \bar{D}^0 D^0 K^+$ are shown in Fig. 2. The known amplitudes that could give a contribution in the Dalitz plot for both modes are

- (i) nonresonant events,
- (ii) the $D_{s1}^*(2700)^+$ meson, and
- (iii) the $D_{s2}^*(2573)^+$ meson, which can decay to $D^0 K^+$, but has not been observed in $B \rightarrow \bar{D}^{(*)} DK$ decays.

The $D_{sJ}^*(2860)^+$ state decays also to $D^0 K^+$ but is not included in the nominal fit. Furthermore, for the mode $B^+ \rightarrow \bar{D}^0 D^0 K^+$, additional contributions from charmonium states are possible and are included in the fit:

- (i) the $\psi(3770)$ meson, and
- (ii) the $\psi(4160)$ meson.

The $\chi_{c2}(2P)$, $\psi(4040)$, and $\psi(4415)$ mesons can also decay to $\bar{D}^0 D^0$. However, they are not included in the nominal fit and are treated separately. In the following fits, the masses and widths of the resonances are fixed to their world averages [16], except for the $D_{s1}^*(2700)^+$ where the parameters are free to vary. The spin of this resonance is assumed to be 1.

1. Preliminary fits

We start by a fit to the Dalitz plot with the previously listed amplitudes in the decays $B^0 \rightarrow D^- D^0 K^+$ and $B^+ \rightarrow \bar{D}^0 D^0 K^+$. The projections on the $D^0 K^+$ invariant mass are shown in Fig. 3 (no nonresonant component is included for $B^+ \rightarrow \bar{D}^0 D^0 K^+$ as explained below). We see

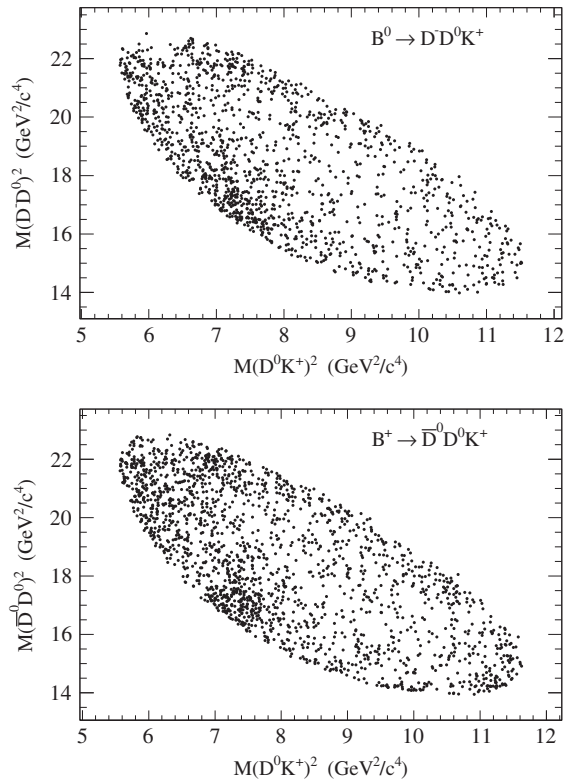


FIG. 2. Distributions of the data for the Dalitz plot for $B^0 \rightarrow D^- D^0 K^+$ (top) and $B^+ \rightarrow \bar{D}^0 D^0 K^+$ (bottom), where each dot represents a B candidate.

clearly in both cases that the fits are not satisfactory, with values of χ^2/n_{dof} (of $\Delta\mathcal{F}$) equal to 82/48 (36) and 265/51 (223) for $B^0 \rightarrow D^- D^0 K^+$ and $B^+ \rightarrow \bar{D}^0 D^0 K^+$, respectively. In particular, we see that the $D^0 K^+$ region between 2350 and 2500 MeV/c^2 is not well described, especially for $B^+ \rightarrow \bar{D}^0 D^0 K^+$. This region corresponds to the threshold in the $D^0 K^+$ phase space. The Belle experiment has also reported this enhancement of data with respect to the

background in the study of the $B^+ \rightarrow \bar{D}^0 D^0 K^+$ decay mode [4].

2. $D^0 K^+$ low-mass excess

We check that the enhancement is due to the signal and not the background using two methods to subtract the background. The first method consists of dividing the $D^0 K^+$ invariant mass range into 20 MeV/c^2 slices and fitting the m_{ES} distribution in each slice. The signal contribution is extracted from the fit and plotted as a function of mass to obtain a background subtracted $D^0 K^+$ invariant mass distribution. The second method is based on the use of the *sPlot* technique [22], which allows the subtraction of the background in the invariant mass distribution using other uncorrelated variables so that the signal is kept with the correct statistical significance for the variable to be plotted. The *sPlot* technique uses the results of the m_{ES} fit described in Sec. III (yields and covariance matrix) and the PDFs of this fit to compute an event-by-event weight for the signal and background categories. We obtain a $D^0 K^+$ invariant mass distribution free of background by applying the *sPlot* weight to each event. Using these two methods of background subtraction, we observe that the enhancement at low mass is present in the $D^0 K^+$ invariant mass distributions for both modes, proving that it originates from $B \rightarrow \bar{D} D^0 K^+$ final states.

We verify that this effect cannot be explained by the reflection of a known resonance. A reflection could originate from cross-feed events. If one of the cross-feed modes of the mode of interest contains a resonance, then this resonance can appear as a structure in the mode of interest, with a smaller magnitude and a shifted mass. As noted earlier, we observe that the cross feed is small for the modes $B^0 \rightarrow D^- D^0 K^+$ and $B^+ \rightarrow \bar{D}^0 D^0 K^+$. We use simulations of $B \rightarrow \bar{D} D_{s1}(2536)$, followed by $D_{s1}(2536) \rightarrow D^* K$, using the branching fractions from Ref. [2] to estimate the possible pollution from these cross-feed

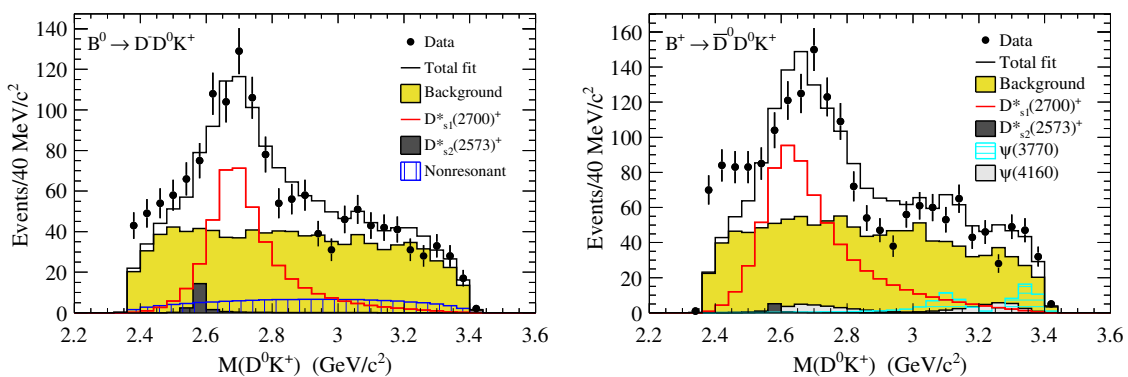


FIG. 3 (color online). Projections of the Dalitz plot on the $D^0 K^+$ axis for the data (dots) and for the result of the preliminary fit (total histogram) for the modes $B^0 \rightarrow D^- D^0 K^+$ (left) and $B^+ \rightarrow \bar{D}^0 D^0 K^+$ (right). The fit includes the background (plain yellow histogram), the nonresonant (vertical-hatched blue histogram), the $D_{s1}^*(2700)^+$ (red histogram), and the $D_{s2}^*(2573)^+$ (plain dark gray histogram) amplitudes. For $B^+ \rightarrow \bar{D}^0 D^0 K^+$, the additional charmonium contributions consist of the $\psi(3770)$ (horizontal-hatched light blue histogram) and the $\psi(4160)$ (plain light gray histogram) amplitudes.

modes. We observe that this source of pollution is negligible and cannot explain the enhancement. We also make use of simulations of the cross-feed processes $B \rightarrow \bar{D}D_{s1}^*(2700)^+$, followed by $D_{s1}^*(2700)^+ \rightarrow D^{(*)}K$, but we observe that these modes give almost no contribution to $B^0 \rightarrow D^-D^0K^+$ and $B^+ \rightarrow \bar{D}^0D^0K^+$. In conclusion, no reflection seems to explain the enhancement seen at low mass in the D^0K^+ invariant mass distributions.

This excess at low mass could be explained by an additional resonance, although none is expected in this mass range. To test this hypothesis, we refit the data adding the PDF of a scalar resonance with mass and width that are free to float. The quality of the fits improves after the addition of the scalar, with values of χ^2/n_{dof} (of $\Delta\mathcal{F}$) equal to 58/44 (-2) and 90/49 (-1) for $B^0 \rightarrow D^-D^0K^+$ and $B^+ \rightarrow \bar{D}^0D^0K^+$, respectively. The fit for $B^0 \rightarrow D^-D^0K^+$ returns a mass and width of the scalar of 2412 ± 16 MeV/ c^2 and 163 ± 64 MeV and for $B^+ \rightarrow \bar{D}^0D^0K^+$ of 2453 ± 20 MeV/ c^2 and 283 ± 45 MeV, respectively (statistical uncertainties only). These two results are not incompatible ($\sim 1.5\sigma$ difference for both mass and width, where σ is the standard deviation), but the assumption of such a wide resonance at this mass would be speculative. We also try fits with a wide virtual resonance below the D^0K^+ threshold, but these fits yield widths with uncertainties that are larger than the corresponding central values. Thus, it is not possible to conclude that a real scalar resonance contributes to the $B \rightarrow \bar{D}D^0K^+$ decays. The excess at low mass, although evident, lacks enough statistics to draw definitive conclusions about its nature. In consequence, since the excess at low D^0K^+ mass in this data is not understood, we use an arbitrary function to describe it.

This function is chosen to be an exponential starting at the D^0K^+ mass threshold. The exponential function takes the form $A_{\text{Expo}} = e^{-\alpha(m_2^2 - m_{2\text{thr}}^2)}$ where A_{Expo} is the amplitude from Eq. (3), α is a free parameter, m_2 the D^0K^+ invariant mass of the event, and $m_{2\text{thr}}$ the mass threshold, corresponding to the sum of the D^0 and K^+ masses. Another approach, introduced in Ref. [23], consists of integrating an exponential contribution as part of the nonresonant amplitude, assuming that the nonresonant amplitude is not necessarily constant over the Dalitz plot.

3. Nominal fits

For $B^0 \rightarrow D^-D^0K^+$, the nominal content of the fit includes the nonresonant, the $D_{s1}^*(2700)^+$, the $D_{s2}^*(2573)^+$, and the exponential amplitudes, which makes a total of nine free parameters in the fit. For $B^+ \rightarrow \bar{D}^0D^0K^+$ the fits are not improved when adding the nonresonant component, so we use for the nominal content of the fit the $D_{s1}^*(2700)^+$, the $D_{s2}^*(2573)^+$, the $\psi(3770)$, the $\psi(4160)$, and the exponential amplitudes. This fit has a total of 11 free parameters.

As stated above, the final fits for $B^0 \rightarrow D^-D^0K^+$ and $B^+ \rightarrow \bar{D}^0D^0K^+$ are each chosen from among 250 fits with

randomized initial values of the fit parameters. For $B^0 \rightarrow D^-D^0K^+$, we observe that the majority of the fits (60%) converge to the exact same values of the set of fitted parameters, which we choose as our nominal fit. However a proportion of fits (23%) converges to a slightly lower value of \mathcal{F} with a sum of fit fractions [Eq. (8)] greater than 250%. This large sum of fractions, which is unlikely to be physical, originates from large interference between the nonresonant and the exponential contributions, which are both *ad hoc* amplitudes. These fits return values of the parameter related to the resonances very close to those of the nominal fit: these differences are taken into account in the calculation of the systematic uncertainties. Moreover, we find a local minimum for 3% of the fits with $\Delta\mathcal{F} = 1$, which we account for in the systematic uncertainties. We observe that 5% of the fits have $\Delta\mathcal{F} > 20$. For $B^+ \rightarrow \bar{D}^0D^0K^+$, one-third of the 250 fits converge to the global minimum, chosen as our nominal fit. We observe four local minima, representing a proportion of 42% of the fits, situated at $\Delta\mathcal{F} < 4$ of the global minimum. Since these fits are close to the nominal one, we use them as a contribution to the systematic uncertainties for the parameters related to the resonances. We see that 10% of the fits have $\Delta\mathcal{F} > 20$, justifying the use of the procedure of randomizing the initial values of the parameters.

The nominal fit for $B^0 \rightarrow D^-D^0K^+$ is shown in Fig. 4 and returns $\chi^2/n_{\text{dof}} = 56/45$. The nominal fit for $B^+ \rightarrow \bar{D}^0D^0K^+$ is presented in Fig. 4 and gives $\chi^2/n_{\text{dof}} = 86/48$. The high value of the χ^2/n_{dof} can be partly explained by some discrepancies between the data and our fit located mainly in the $\psi(3770)$ region. We do not extract any information from this region, and we consider that the fit gives a satisfactory description of the data in other regions.

To assess the values found for \mathcal{F} for the nominal fit for each mode, we generate a large number of Monte Carlo samples based on the PDFs of the nominal fits with the statistics of the data and fit these samples with the same method as in the data. We observe that the nominal values of \mathcal{F} for the two modes are close (0.2σ) to the central values of the distributions of \mathcal{F} obtained from the Monte Carlo samples. Similarly to the data, the simulations show the presence of several local minima close to the global minimum.

Comparing the fit results before and after removing a resonance with fixed shape parameters allows us to translate directly the difference of negative log likelihood as a χ^2 distribution with two degrees of freedom (modulus and phase). A difference $\Delta\mathcal{F}$ of 12 and 29 corresponds roughly to a statistical significance of 3σ and 5σ , respectively. This significance does not take into account the systematic uncertainties, and the final significance decreases after taking them into account. This property is used here to estimate the need for the $D_{s2}^*(2573)^+$ and $\psi(4160)$ resonances. In a first stage, we repeat the nominal fit without the $D_{s2}^*(2573)^+$ amplitude. We observe that the minimum log

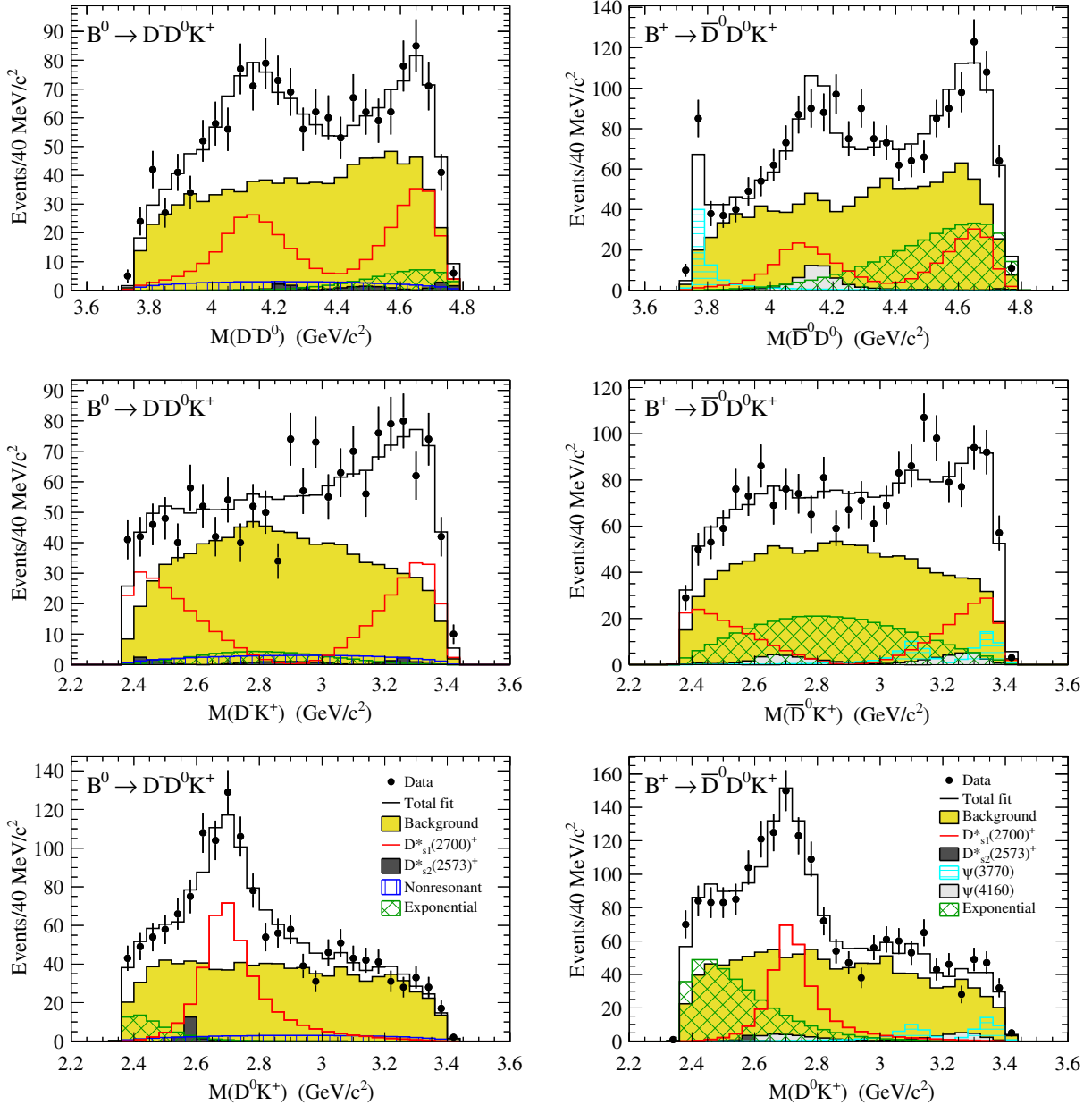


FIG. 4 (color online). Projections of the Dalitz plot on the three axes for the data (dots) and for the result of the nominal fit (total histogram) for the modes $B^0 \rightarrow D^- D^0 K^+$ (left) and $B^+ \rightarrow \bar{D}^0 D^0 K^+$ (right). The fit includes the background (plain yellow histogram), the nonresonant (vertical-hatched blue histogram), present only for $B^0 \rightarrow D^- D^0 K^+$, the $D_{s1}^*(2700)^+$ (red histogram), the $D_{s2}^*(2573)^+$ (plain dark gray histogram), and the exponential (cross-hatched green histogram) amplitudes. For $B^+ \rightarrow \bar{D}^0 D^0 K^+$, the additional charmonium contributions consist of the $\psi(3770)$ (horizontal-hatched light blue histogram) and the $\psi(4160)$ (plain light gray histogram) amplitudes.

likelihood increases with $\Delta\mathcal{F} = 16$ for $B^0 \rightarrow D^- D^0 K^+$ and $\Delta\mathcal{F} = 5$ for $B^+ \rightarrow \bar{D}^0 D^0 K^+$, indicating that the presence of the $D_{s2}^*(2573)^+$ resonance is significant in $B^0 \rightarrow D^- D^0 K^+$. Removing the $\psi(4160)$ component from the Dalitz plot fit of $B^+ \rightarrow \bar{D}^0 D^0 K^+$ gives $\Delta\mathcal{F} = 23$.

Adding an additional amplitude for either the $D_{sJ}^*(2860)^+$ or the $D_{sJ}^*(3040)^+$ resonance does not improve the fits (assuming a spin of 1 for these two states). For $B^+ \rightarrow \bar{D}^0 D^0 K^+$, adding a contribution for either the

$\chi_{c2}(2P)$, $\psi(4040)$, or $\psi(4415)$ meson does not improve the fit to a significant level. None of the parameters changed by a statistically significant amount when adding to the fit these extra resonances, and no systematic error is assigned for these resonances.

V. SYSTEMATIC UNCERTAINTIES

We consider several sources of systematic uncertainties in the fit parameters, such as the moduli, the phases, the fit

TABLE I. Systematic uncertainties for $B^0 \rightarrow D^- D^0 K^+$ in the moduli, in the phases ($^\circ$), in the fractions (%), in the mass (MeV/c^2) and the width (MeV) of the $D_{s1}^*(2700)^+$, and in α , the parameter of the exponential function. The labels refer to systematic uncertainties related to the fit bias (“Bias”), efficiency interpolation (“Eff.”), statistical uncertainty in efficiency (“Eff. II”), background knowledge (“Bkg”), Blatt-Weisskopf barrier (“BW”), low-mass description (“Low mass”), $D_{s2}^*(2573)^+$ amplitude (“ D_{s2}^* ”), and other minima (“Min.”). The sign ‘—’ means that no systematic uncertainty has been attributed to the specific parameter.

| Parameter | Value | Bias | Eff. | Eff. II | Bkg | BW | Low mass | D_{s2}^* | Min. | Total |
|-----------------------------|-------|-------------|------------|-------------|--------------------|--------------------|------------------|------------|------------------|--------------------|
| Modulus $D_{s2}^*(2573)^+$ | 0.031 | ± 0.001 | 0 | ± 0.001 | 0 | ± 0.001 | 0 | 0 | ± 0.001 | ± 0.002 |
| Modulus nonresonant | 1.33 | ± 0.09 | ± 0.03 | ± 0.05 | $^{+0.21}_{-0.33}$ | $^{+0.39}_{-0.00}$ | 0 | +0.04 | — | $^{+0.46}_{-0.35}$ |
| Modulus exponential | 6.94 | ± 0.24 | ± 0.06 | ± 0.19 | $^{+0.12}_{-0.21}$ | $^{+0.72}_{-0.20}$ | 0 | +0.21 | — | $^{+0.82}_{-0.43}$ |
| Phase $D_{s2}^*(2573)^+$ | 277 | ± 4 | ± 1 | ± 2 | ± 2 | $^{+0}_{-8}$ | $^{+2}_{-0}$ | 0 | $^{+4}_{-0}$ | $^{+6}_{-9}$ |
| Phase nonresonant | 287 | ± 2 | 0 | ± 1 | $^{+9}_{-6}$ | $^{+2}_{-14}$ | 0 | 0 | — | $^{+10}_{-15}$ |
| Phase exponential | 269 | ± 6 | ± 1 | ± 4 | $^{+3}_{-0}$ | $^{+0}_{-13}$ | 0 | +15 | — | $^{+17}_{-15}$ |
| Fraction $D_{s1}^*(2700)^+$ | 66.7 | — | ± 0.2 | ± 0.6 | $^{+2.2}_{-2.1}$ | $^{+0.4}_{-2.1}$ | $^{+1.3}_{-0.0}$ | +0.6 | $^{+2.3}_{-2.3}$ | $^{+3.5}_{-3.8}$ |
| Fraction $D_{s2}^*(2573)^+$ | 3.2 | — | 0 | ± 0.2 | $^{+0.0}_{-0.1}$ | $^{+0.0}_{-0.3}$ | $^{+0.2}_{-0.0}$ | 0 | $^{+0.1}_{-0.0}$ | $^{+0.3}_{-0.4}$ |
| Fraction nonresonant | 10.9 | — | ± 0.3 | ± 0.7 | $^{+3.3}_{-4.3}$ | $^{+6.1}_{-0.0}$ | 0 | +0.2 | — | $^{+7.0}_{-4.3}$ |
| Fraction exponential | 9.9 | — | ± 0.2 | ± 0.5 | $^{+2.9}_{-1.5}$ | $^{+0.0}_{-2.9}$ | 0 | +0.9 | — | $^{+3.0}_{-3.3}$ |
| $M(D_{s1}^*(2700)^+)$ | 2694 | ± 2 | 0 | ± 1 | 0 | $^{+13}_{-2}$ | $^{+0}_{-1}$ | 0 | $^{+3}_{0}$ | $^{+13}_{-3}$ |
| $\Gamma(D_{s1}^*(2700)^+)$ | 145 | ± 8 | ± 1 | ± 3 | $^{+4}_{-3}$ | $^{+17}_{-9}$ | $^{+5}_{-0}$ | -6 | $^{+11}_{-4}$ | $^{+22}_{-14}$ |
| α | 1.43 | ± 0.11 | ± 0.02 | ± 0.08 | $^{+0.20}_{-0.26}$ | $^{+0.48}_{-0.00}$ | 0 | -0.06 | — | $^{+0.54}_{-0.30}$ |

fractions, and the mass and width of the $D_{s1}^*(2700)^+$. Tables I and II give the details of the systematic uncertainties. To estimate a potential fit bias, we generate a large number of Monte Carlo samples based on the nominal fits

with the same statistics as in the data. We perform the Dalitz plot fit on these samples and extract the central value and uncertainty of each parameter. We obtain a distribution of the pull for each parameter, defined as the difference

TABLE II. Systematic uncertainties for $B^+ \rightarrow \bar{D}^0 D^0 K^+$ in the moduli, in the phases ($^\circ$), in the fractions (%), in the mass (MeV/c^2) and the width (MeV) of the $D_{s1}^*(2700)^+$, and in α , the parameter of the exponential function. The labels refer to systematic uncertainties related to the fit bias (“Bias”), efficiency interpolation (“Eff.”), statistical uncertainty in efficiency (“Eff. II”), background knowledge (“Bkg”), Blatt-Weisskopf barrier (“BW”), low-mass description (“Low mass”), $D_{s2}^*(2573)^+$ amplitude (“ D_{s2}^* ”), $\psi(3770)$ amplitude (“ ψ ”), and other minima (“Min.”). The sign ‘—’ means that no systematic uncertainty has been attributed to the specific parameter.

| Parameter | Value | Bias | Eff. | Eff. II | Bkg | BW | Low mass | D_{s2}^* | ψ | Min. | Total |
|-----------------------------|-------|-------------|-------------|-------------|--------------------|----------------------|----------------------|------------|--------|----------------------|----------------------|
| Modulus $D_{s2}^*(2573)^+$ | 0.021 | ± 0.001 | ± 0.001 | ± 0.001 | 0 | $^{+0.003}_{-0.000}$ | $^{+0.006}_{-0.000}$ | 0 | 0 | $^{+0.005}_{-0.002}$ | $^{+0.009}_{-0.003}$ |
| Modulus $\psi(3770)$ | 1.40 | ± 0.08 | ± 0.02 | ± 0.03 | $^{+0.05}_{-0.06}$ | $^{+0.03}_{-0.10}$ | $^{+0.06}_{-0.00}$ | +0.07 | -0.19 | $^{+0.14}_{-0.00}$ | $^{+0.20}_{-0.24}$ |
| Modulus $\psi(4160)$ | 0.78 | ± 0.02 | ± 0.01 | ± 0.03 | ± 0.01 | $^{+0.00}_{-0.10}$ | $^{+0.16}_{-0.00}$ | +0.06 | -0.02 | $^{+0.06}_{-0.08}$ | $^{+0.18}_{-0.14}$ |
| Modulus exponential | 16.15 | ± 0.53 | ± 0.13 | ± 0.35 | $^{+0.57}_{-0.70}$ | $^{+0.00}_{-1.44}$ | 0 | +0.66 | -0.18 | — | $^{+1.09}_{-1.74}$ |
| Phase $D_{s2}^*(2573)^+$ | 267 | ± 9 | ± 3 | ± 3 | $^{+7}_{-8}$ | $^{+1}_{-3}$ | $^{+5}_{-0}$ | 0 | 0 | $^{+10}_{-0}$ | $^{+17}_{-13}$ |
| Phase $\psi(3770)$ | 284 | ± 5 | 0 | ± 2 | ± 1 | $^{+0}_{-22}$ | $^{+7}_{-19}$ | -2 | -4 | $^{+25}_{-4}$ | $^{+26}_{-30}$ |
| Phase $\psi(4160)$ | 188 | ± 6 | 0 | ± 2 | ± 4 | $^{+0}_{-3}$ | $^{+12}_{-0}$ | -1 | +1 | $^{+2}_{-15}$ | $^{+14}_{-17}$ |
| Phase exponential | 308 | ± 2 | ± 1 | ± 2 | ± 2 | ± 4 | 0 | +2 | +1 | — | $^{+6}_{-5}$ |
| Fraction $D_{s1}^*(2700)^+$ | 38.3 | — | ± 0.3 | ± 0.6 | $^{+0.3}_{-0.0}$ | $^{+0.0}_{-0.1}$ | $^{+0.0}_{-2.4}$ | -1.4 | 0 | $^{+0.0}_{-5.5}$ | $^{+0.8}_{-6.2}$ |
| Fraction $D_{s2}^*(2573)^+$ | 0.6 | — | ± 0.1 | ± 0.1 | 0 | $^{+0.2}_{-0.0}$ | $^{+0.3}_{-0.0}$ | 0 | 0 | $^{+0.2}_{-0.1}$ | $^{+0.4}_{-0.2}$ |
| Fraction $\psi(3770)$ | 9.0 | — | 0 | ± 0.3 | $^{+0.3}_{-0.2}$ | $^{+0.0}_{-0.5}$ | $^{+0.1}_{-0.4}$ | +0.1 | -0.4 | ± 0.1 | $^{+0.4}_{-0.8}$ |
| Fraction $\psi(4160)$ | 6.4 | — | ± 0.1 | ± 0.3 | ± 0.3 | $^{+0.0}_{-0.7}$ | $^{+1.7}_{-0.1}$ | +0.4 | -0.1 | $^{+0.7}_{-2.3}$ | $^{+1.9}_{-2.4}$ |
| Fraction exponential | 44.5 | — | ± 0.2 | ± 0.6 | $^{+0.0}_{-0.2}$ | $^{+0.0}_{-2.0}$ | 0 | +1.1 | -0.2 | — | $^{+1.3}_{-2.1}$ |
| $M(D_{s1}^*(2700)^+)$ | 2707 | ± 4 | 0 | ± 1 | ± 3 | $^{+7}_{-4}$ | $^{+0}_{-4}$ | +1 | 0 | $^{+0}_{-5}$ | ± 8 |
| $\Gamma(D_{s1}^*(2700)^+)$ | 113 | ± 5 | ± 1 | ± 3 | $^{+9}_{-7}$ | $^{+17}_{-0}$ | $^{+0}_{-9}$ | -5 | +2 | $^{+0}_{-7}$ | $^{+20}_{-16}$ |
| α | 0.68 | ± 0.01 | 0 | ± 0.01 | ± 0.01 | $^{+0.02}_{-0.00}$ | 0 | -0.02 | 0 | — | ± 0.02 |

between the central value from a particular Monte Carlo sample and the nominal value, divided by the uncertainty in the fit value from the Monte Carlo sample. These distributions have a width compatible with 1 as expected, but their mean is observed to be shifted with respect to 0, which points toward fit biases that we correct for in our results. The systematic uncertainty related to this bias correction is taken as half of the bias added in quadrature with the uncertainty in the bias (the systematic uncertainty related to the bias is labeled as “Bias” in Tables I and II).

Systematic uncertainties arise from the efficiency calculation. To estimate these we first use the raw efficiency in each bin of the Dalitz plot instead of the interpolation and consider the difference for each parameter as an estimate of the systematic uncertainties for the efficiency (labeled as “Eff.” in Tables I and II). Second, we take into account the statistical fluctuation on the efficiency due to the finite number of Monte Carlo events. In each bin of the Dalitz plot, we randomize the efficiency within its statistical uncertainty and produce many new mappings of the efficiency. The analysis is performed using these new efficiency mappings, which gives a distribution for each parameter from which we extract the systematic uncertainties (column “Eff. II”).

Another source of systematic uncertainty comes from the background description. Repeating the analysis using the raw value of the background in each bin of the Dalitz plot instead of the interpolation does not change the results. In addition, the signal purity is varied according to its total uncertainty (see Sec. III), which allows us to get the systematic uncertainty related to the signal and background knowledge (column “Bkg”).

Several systematic uncertainties arise from the fit modeling. The first one comes from the Blatt-Weisskopf barrier, which is not known precisely. Fits of both modes with this value as a free parameter show that the analysis is not sensitive to it. To estimate the related systematic uncertainty, we repeat the analysis changing the value of the Blatt-Weisskopf barrier radius from the nominal value 1.5 GeV^{-1} to 5 GeV^{-1} and 0 GeV^{-1} . The differences for each parameter between the nominal fit and these fits give the systematic uncertainties (labeled as “BW” in the tables). Another systematic uncertainty originates from the description of the low-mass excess. Since this effect is not understood in the current data, it is important to estimate the possible influence it induces on the fit parameters, especially the mass and the width of the $D_{s1}^*(2700)^+$ meson. To compute the systematic uncertainties associated with this effect, we assume first that the excess originates from a scalar resonance at low mass: we repeat the fits replacing the exponential contribution by a scalar resonance with a mass and a width free to float. Second, instead of the exponential function, we use an alternative model, $A_{\text{Alt}} = \frac{1}{1+a \times (m_2^2 - m_{2\text{thr}}^2)}$ with a a free parameter. The maximum deviations with respect to the nominal fit for each of these

two alternatives are used as the systematic uncertainties (column “Low mass”). We then study the influence of the resonances on the analyses. Since the $D_{s2}^*(2573)^+$ amplitude presents a low fit fraction, we repeat the fits without this amplitude and take the difference as a systematic uncertainty (column “ D_{s2}^* ”). The effect of the spin-1 $D_{sJ}^*(2860)^+$ has also been investigated: because the fits return negligible fractions for this state, the systematic uncertainties on the other parameters are found to be negligible. For $B^+ \rightarrow \bar{D}^0 D^0 K^+$, another systematic uncertainty (column “ ψ ”) arises from the $\psi(3770)$ parameters fixed to the world average value [16]. As an alternative, we use the measurement from the KEDR experiment [24]. This experiment reports a result which takes into account the resonance-continuum interference in the near-threshold region and which agrees well with previous *BABAR* measurements [2,25].

As discussed previously, 250 fits are performed for each mode with randomized initial values of the fit parameters, which allows us to find the nominal fit. We find several minima which are close to the nominal fit, and we use the largest differences in parameter values (for those related to resonances) as contributions to their systematic uncertainties (column “Min.”).

VI. RESULTS

A. Dalitz plot analysis

The results for the Dalitz plot analysis of the modes $B^0 \rightarrow D^- D^0 K^+$ and $B^+ \rightarrow \bar{D}^0 D^0 K^+$ are presented in Tables III and IV. In both modes, we observe a large contribution of the $D_{s1}^*(2700)^+$ resonance via $B^0 \rightarrow D^- D_{s1}^*(2700)^+, D_{s1}^*(2700)^+ \rightarrow D^0 K^+$ for $B^0 \rightarrow D^- D^0 K^+$ and via $B^+ \rightarrow \bar{D}^0 D_{s1}^*(2700)^+, D_{s1}^*(2700)^+ \rightarrow D^0 K^+$ for $B^+ \rightarrow \bar{D}^0 D^0 K^+$. This is the first time the $D_{s1}^*(2700)^+$ is observed in the decay $B^0 \rightarrow D^- D^0 K^+$. We observe that the $D_{s2}^*(2573)^+$ meson contributes a small fraction to $B^0 \rightarrow D^- D^0 K^+$ whereas it is not significant in the other mode. We note that the $D_{s2}^*(2573)^+$ meson is expected to be

TABLE III. Results from the Dalitz plot fit (moduli, phases, and fractions) for $B^0 \rightarrow D^- D^0 K^+$. The different contributions are listed: the $D_{s1}^*(2700)^+$ and $D_{s2}^*(2573)^+$ resonances, the non-resonant amplitude, and the low-mass excess described by an exponential. The first uncertainties are statistical and the second systematic.

| Contribution | Modulus | Phase (\circ) | Fraction (%) |
|--------------------|----------------------------------|--------------------------|-------------------------------|
| $D_{s1}^*(2700)^+$ | 1.00 | 0 | $66.7 \pm 7.8^{+3.5}_{-3.8}$ |
| $D_{s2}^*(2573)^+$ | 0.031 ± 0.008 ± 0.002 | $277 \pm 17^{+6}_{-9}$ | $3.2 \pm 1.6^{+0.3}_{-0.4}$ |
| Nonresonant | $1.33 \pm 0.63^{+0.46}_{-0.35}$ | $287 \pm 21^{+10}_{-15}$ | $10.9 \pm 6.6^{+7.0}_{-4.3}$ |
| Exponential | $6.94 \pm 1.83^{+0.82}_{-0.43}$ | $269 \pm 33^{+17}_{-15}$ | $9.9 \pm 2.9^{+3.0}_{-3.3}$ |
| Sum | | | $90.6 \pm 10.7^{+8.4}_{-6.7}$ |

TABLE IV. Results from the Dalitz plot fit (moduli, phases, and fractions) for $B^+ \rightarrow \bar{D}^0 D^0 K^+$. The different contributions are listed: the $D_{s1}^*(2700)^+$, $D_{s2}^*(2573)^+$, $\psi(3770)$, and $\psi(4160)$ resonances, and the low-mass excess described by an exponential. The first uncertainties are statistical and the second systematic.

| Contribution | Modulus | Phase ($^\circ$) | Fraction (%) |
|--------------------|-------------------------------------|--------------------------|------------------------------|
| $D_{s1}^*(2700)^+$ | 1.00 | 0 | $38.3 \pm 5.0^{+0.8}_{-6.2}$ |
| $D_{s2}^*(2573)^+$ | $0.021 \pm 0.010^{+0.009}_{-0.003}$ | $267 \pm 30^{+17}_{-13}$ | $0.6 \pm 1.1^{+0.4}_{-0.2}$ |
| $\psi(3770)$ | $1.40 \pm 0.21^{+0.20}_{-0.24}$ | $284 \pm 22^{+26}_{-30}$ | $9.0 \pm 3.1^{+0.4}_{-0.8}$ |
| $\psi(4160)$ | $0.78 \pm 0.20^{+0.18}_{-0.14}$ | $188 \pm 13^{+14}_{-17}$ | $6.4 \pm 3.1^{+1.9}_{-2.4}$ |
| Exponential | $16.15 \pm 2.26^{+1.09}_{-1.74}$ | $308 \pm 8^{+6}_{-5}$ | $44.5 \pm 6.2^{+1.3}_{-2.1}$ |
| Sum | | | $98.9 \pm 9.2^{+2.5}_{-7.0}$ |

suppressed in $B \rightarrow \bar{D}^{(*)} D^{(*)} K$ decays due to its spin value of 2. We observe the decay $B^+ \rightarrow \psi(3770)K^+$, $\psi(3770) \rightarrow \bar{D}^0 D^0$, which confirms one of our previous results [2]. We notice that the process $B^+ \rightarrow \psi(4160)K^+$ followed by $\psi(4160) \rightarrow \bar{D}^0 D^0$ is needed to improve the description of the data. The low-mass excess in the $D^0 K^+$ invariant mass is evident in $B^0 \rightarrow D^- D^0 K^+$ and is the main contribution in $B^+ \rightarrow \bar{D}^0 D^0 K^+$. With this data sample it is not possible to determine the origin of this excess. The exponential function used to describe the effect has a parameter α equal to $1.43 \pm 0.71^{+0.54}_{-0.30}$ and $0.68 \pm 0.08 \pm 0.02$ for $B^0 \rightarrow D^- D^0 K^+$ and $B^+ \rightarrow \bar{D}^0 D^0 K^+$, respectively.

B. Branching fractions

The partial branching fraction \mathcal{B}_{res} for a given resonance is computed using the fraction f_{res} of the resonance (see Tables III and IV) and the total branching fraction \mathcal{B}_{tot} of the specific B mode. We use the total branching fractions measured in a previous publication [15] with the exact same data sample. The computation is as follows:

$$\mathcal{B}_{\text{res}} = f_{\text{res}} \times \mathcal{B}_{\text{tot}}.$$

The uncertainties for the partial branching fraction are computed from the quadratic sum of the uncertainties from the total branching fraction [15] and the uncertainties from the fraction (see Tables III and IV), where we treat separately the statistical and systematic uncertainties.

The results are presented in Table V. We can compare these results with previous publications that are available for the mode $B^+ \rightarrow \bar{D}^0 D^0 K^+$. In *BABAR* [2], using an analysis of the $\bar{D}^0 D^0$ invariant mass, the result for the $\psi(3770)$ was $\mathcal{B}(B^+ \rightarrow \psi(3770)K^+[\bar{D}^0 D^0]) = (1.41 \pm 0.30 \pm 0.22) \times 10^{-4}$, which is in good agreement with the current result. This present measurement supersedes the previous one. The Belle experiment [4] finds for the partial branching fraction $\mathcal{B}(B^+ \rightarrow \bar{D}^0 D_{s1}^*(2700)^+ [D^0 K^+]) = (11.3 \pm 2.2^{+1.4}_{-2.8}) \times 10^{-4}$ and $\mathcal{B}(B^+ \rightarrow \psi(3770)K^+[\bar{D}^0 D^0]) = (2.2 \pm 0.5 \pm 0.3) \times 10^{-4}$, which present a difference with our measurements of 1.7σ and 1.4σ , respectively.

TABLE V. Summary of partial branching fractions. The first uncertainties are statistical and the second systematic. The notation $B^0 \rightarrow D^- D_{s1}^*(2700)^+ [D^0 K^+]$ refers to $B^0 \rightarrow D^- D_{s1}^*(2700)^+$ followed by $D_{s1}^*(2700)^+ \rightarrow D^0 K^+$.

| Mode | \mathcal{B} (10^{-4}) |
|--|-----------------------------|
| $B^0 \rightarrow D^- D_{s1}^*(2700)^+ [D^0 K^+]$ | $7.14 \pm 0.96 \pm 0.69$ |
| $B^+ \rightarrow \bar{D}^0 D_{s1}^*(2700)^+ [D^0 K^+]$ | $5.02 \pm 0.71 \pm 0.93$ |
| $B^0 \rightarrow D^- D_{s2}^*(2573)^+ [D^0 K^+]$ | $0.34 \pm 0.17 \pm 0.05$ |
| $B^+ \rightarrow \bar{D}^0 D_{s2}^*(2573)^+ [D^0 K^+]$ | $0.08 \pm 0.14 \pm 0.05$ |
| $B^+ \rightarrow \psi(3770)K^+ [\bar{D}^0 D^0]$ | $1.18 \pm 0.41 \pm 0.15$ |
| $B^+ \rightarrow \psi(4160)K^+ [\bar{D}^0 D^0]$ | $0.84 \pm 0.41 \pm 0.33$ |

The significance of the decay of the $\psi(4160)$ charmonium resonance to $\bar{D}^0 D^0$ is 3.3σ , including systematic uncertainties. The significance of the $D_{s2}^*(2573)^+$ meson decay to $D^0 K^+$ is 3.4σ (for the mode $B^0 \rightarrow D^- D^0 K^+$), including systematic uncertainties.

C. Properties of $D_{s1}^*(2700)^+$

We show in Table VI the result for the mass and width of the $D_{s1}^*(2700)^+$ meson for the two modes obtained from the Dalitz plot analysis. The measurements in the two final states agree with each other within their uncertainties. We combine the measurements for the mass and width, respectively, calculating the weighted means and taking into account the asymmetric uncertainties. This procedure works for uncertainties that are not correlated between the measurements. Only the systematic uncertainty coming from the Blatt-Weisskopf factor is correlated between the modes: we perform first the combination without this particular systematic uncertainty, where we obtain $M(D_{s1}^*(2700)^+) = 2699 \pm 7 \text{ MeV}/c^2$ and $\Gamma(D_{s1}^*(2700)^+) = 127 \pm 17 \text{ MeV}$ (including statistical and systematic). For the uncertainty related to the Blatt-Weisskopf factor, we use the maximum positive and negative deviations found in the two modes that we add quadratically to the total uncertainties.

Finally, the combination of both modes gives

$$\begin{aligned} M(D_{s1}^*(2700)^+) &= 2699^{+14}_{-7} \text{ MeV}/c^2, \\ \Gamma(D_{s1}^*(2700)^+) &= 127^{+24}_{-19} \text{ MeV}, \end{aligned} \quad (9)$$

where the uncertainties quoted are the total uncertainties (including statistical and systematic).

TABLE VI. Mass and width of the $D_{s1}^*(2700)^+$ meson obtained from the Dalitz plot analyses of the modes $B^0 \rightarrow D^- D^0 K^+$ and $B^+ \rightarrow \bar{D}^0 D^0 K^+$. The first uncertainties are statistical and the second systematic.

| Mode | Mass (MeV/ c^2) | Width (MeV) |
|-------------------------------------|-------------------------|--------------------------|
| $B^0 \rightarrow D^- D^0 K^+$ | $2694 \pm 8^{+13}_{-3}$ | $145 \pm 24^{+22}_{-14}$ |
| $B^+ \rightarrow \bar{D}^0 D^0 K^+$ | $2707 \pm 8 \pm 8$ | $113 \pm 21^{+20}_{-16}$ |

TABLE VII. Value of $\Delta\mathcal{F}$ and χ^2/n_{dof} for the hypotheses $J = 0, 1, 2$ for the two modes. The nominal fit is presented in bold characters.

| Mode | $J = 0$ | | $J = 1$ | $J = 2$ | |
|-------------------------------------|---------------------|-------------------------|-------------------------|---------------------|-------------------------|
| | $\Delta\mathcal{F}$ | χ^2/n_{dof} | χ^2/n_{dof} | $\Delta\mathcal{F}$ | χ^2/n_{dof} |
| $B^0 \rightarrow D^- D^0 K^+$ | 131 | 131/45 | 56/45 | 108 | 125/45 |
| $B^+ \rightarrow \bar{D}^0 D^0 K^+$ | 63 | 137/48 | 86/48 | 99 | 145/48 |

These values can be compared to the current world average of $M(D_{s1}^*(2700)^+) = 2709 \pm 4 \text{ MeV}/c^2$ and $\Gamma(D_{s1}^*(2700)^+) = 117 \pm 13 \text{ MeV}$ [16]. Our measurements are compatible with the world averages.

The Dalitz plot analyses have been performed with the spin hypothesis $J = 1$ for the $D_{s1}^*(2700)^+$. To test this hypothesis, we repeat the fits using the hypotheses $J = 0$ and $J = 2$. The results are presented in Table VII. We conclude from this table that $J = 0, 2$ are not able to fit correctly the data, and that $J = 1$ is strongly favored. Because of parity conservation, we deduce that the $D_{s1}^*(2700)^+$ meson is a state with $J^P = 1^-$, which confirms the measurement performed by the Belle experiment [4].

VII. CONCLUSIONS

We have analyzed 471×10^6 pairs of B mesons recorded by the *BABAR* experiment and studied the decays $B^0 \rightarrow D^- D^0 K^+$ and $B^+ \rightarrow \bar{D}^0 D^0 K^+$. Dalitz plot analyses of these decays have been performed, where we extract moduli and phases for each contribution to these decay modes. We observe the $D_{s1}^*(2700)^+$ meson in both final states and measure its mass and width to be

$$\begin{aligned} M(D_{s1}^*(2700)^+) &= 2699_{-7}^{+14} \text{ MeV}/c^2, \\ \Gamma(D_{s1}^*(2700)^+) &= 127_{-19}^{+24} \text{ MeV}, \end{aligned} \quad (10)$$

where the uncertainties include statistical and systematic uncertainties. We determine its spin parity to be $J^P = 1^-$.

Several possibilities have been discussed to interpret the $D_{s1}^*(2700)^+$ meson. This resonance could be interpreted as the $n^{2S+1}L_J = 1^3D_1 c\bar{s}$ state [26] or as the first radial excitation of the $D_s^*(2112)$ meson (2^3S_1) [27]. Some authors interpret the $D_{s1}^*(2700)^+$ state as a mixing between the 2^3S_1 and the 1^3D_1 states [28], obtaining a model which is able to solve some of the discrepancies with the

experimental data. Another possibility would be that the signal interpreted as the $D_{s1}^*(2700)^+$ originates from two resonances overlapping each other [26].

We observe an enhancement between 2350 and 2500 MeV/c^2 in the $D^0 K^+$ invariant mass that we are not able to interpret. This enhancement, which has an important contribution in the $B^+ \rightarrow \bar{D}^0 D^0 K^+$ decay mode, is described by an *ad hoc* function in the Dalitz plot fit. This effect was also seen in the Belle experiment in the study of the $B^+ \rightarrow \bar{D}^0 D^0 K^+$ final state [4].

It is not clear what could be the cause of this enhancement in the $D^0 K^+$ invariant mass, although we note that some D_s excited states are expected in this mass range in some models [27,29] and have not been observed yet. Some authors, as for example in Ref. [23], who have observed the same effect in other channels claim that it could be a specific form of a nonresonant amplitude.

Finally, we do not observe the $D_{sJ}^*(2860)^+$ and $D_{sJ}(3040)^+$ resonances in the final states $B^0 \rightarrow D^- D^0 K^+$ and $B^+ \rightarrow \bar{D}^0 D^0 K^+$.

ACKNOWLEDGMENTS

We are grateful for the extraordinary contributions of our PEP-II colleagues in achieving the excellent luminosity and machine conditions that have made this work possible. The success of this project also relies critically on the expertise and dedication of the computing organizations that support *BABAR*. The collaborating institutions wish to thank SLAC for its support and the kind hospitality extended to them. This work is supported by the U.S. Department of Energy and National Science Foundation, the Natural Sciences and Engineering Research Council (Canada), the Commissariat à l'Énergie Atomique and Institut National de Physique Nucléaire et de Physique des Particules (France), the Bundesministerium für Bildung und Forschung and Deutsche Forschungsgemeinschaft (Germany), the Istituto Nazionale di Fisica Nucleare (Italy), the Foundation for Fundamental Research on Matter (The Netherlands), the Research Council of Norway, the Ministry of Education and Science of the Russian Federation, Ministerio de Economía y Competitividad (Spain), the Science and Technology Facilities Council (United Kingdom), and the Binational Science Foundation (U.S.-Israel). Individuals have received support from the Marie-Curie IEF program (European Union) and the A. P. Sloan Foundation (USA).

[1] Charge conjugate reactions are assumed throughout this article.

[2] B. Aubert *et al.* (*BABAR* Collaboration), *Phys. Rev. D* **77**, 011102 (2008).

[3] T. Aushev *et al.* (Belle Collaboration), *Phys. Rev. D* **83**, 051102 (2011).

[4] J. Brodzicka *et al.* (Belle Collaboration), *Phys. Rev. Lett.* **100**, 092001 (2008).

- [5] S. Godfrey and N. Isgur, *Phys. Rev. D* **32**, 189 (1985).
- [6] B. Aubert *et al.* (BABAR Collaboration), *Phys. Rev. Lett.* **90**, 242001 (2003); D. Besson *et al.* (CLEO Collaboration), *Phys. Rev. D* **68**, 032002 (2003).
- [7] B. Aubert *et al.* (BABAR Collaboration), *Phys. Rev. Lett.* **97**, 222001 (2006); *Phys. Rev. D* **80**, 092003 (2009).
- [8] R. Aaij *et al.* (LHCb Collaboration), *J. High Energy Phys.* **10** (2012) 151.
- [9] R. Aaij *et al.* (LHCb Collaboration), *Phys. Rev. D* **90**, 072003 (2014); *Phys. Rev. Lett.* **113**, 162001 (2014).
- [10] J. P. Lees *et al.* (BABAR Collaboration), *Nucl. Instrum. Methods Phys. Res., Sect. A* **726**, 203 (2013).
- [11] B. Aubert *et al.* (BABAR Collaboration), *Nucl. Instrum. Methods Phys. Res., Sect. A* **479**, 1 (2002); **729**, 615 (2013).
- [12] D. J. Lange, *Nucl. Instrum. Methods Phys. Res., Sect. A* **462**, 152 (2001).
- [13] T. Sjostrand, S. Mrenna, and P. Skands, *J. High Energy Phys.* **05** (2006) 026.
- [14] S. Agostinelli *et al.* (GEANT4 Collaboration), *Nucl. Instrum. Methods Phys. Res., Sect. A* **506**, 250 (2003).
- [15] P. del Amo Sanchez *et al.* (BABAR Collaboration), *Phys. Rev. D* **83**, 032004 (2011).
- [16] J. Beringer *et al.* (Particle Data Group), *Phys. Rev. D* **86**, 010001 (2012).
- [17] E. D. Bloom and C. Peck, *Annu. Rev. Nucl. Part. Sci.* **33**, 143 (1983).
- [18] H. Albrecht *et al.* (ARGUS Collaboration), *Phys. Lett. B* **241**, 278 (1990).
- [19] S. Kopp *et al.* (CLEO collaboration), *Phys. Rev. D* **63**, 092001 (2001).
- [20] J. M. Blatt and V. F. Weisskopf, *Theoretical Nuclear Physics* (John Wiley & Sons, New York, 1952).
- [21] P. del Amo Sanchez *et al.* (BABAR Collaboration), *Phys. Rev. D* **83**, 052001 (2011).
- [22] M. Pivk and F. R. Le Diberder, *Nucl. Instrum. Methods Phys. Res., Sect. A* **555**, 356, 2005.
- [23] A. Garmash *et al.* (Belle Collaboration), *Phys. Rev. D* **71**, 092003 (2005).
- [24] V. V. Anashin *et al.*, *Phys. Lett. B* **711**, 292 (2012).
- [25] B. Aubert *et al.* (BABAR Collaboration), *Phys. Rev. D* **76**, 111105 (2007).
- [26] S. Godfrey and I. T. Jardine, *Phys. Rev. D* **89**, 074023 (2014).
- [27] B. Chen, D. X. Wang, and A. Zhang, *Phys. Rev. D* **80**, 071502 (2009); P. Colangelo, F. De Fazio, F. Giannuzzi, and S. Nicotri, *Phys. Rev. D* **86**, 054024 (2012).
- [28] D. Li, P. Ji, and B. Ma, *Eur. Phys. J. C* **71**, 1582 (2011).
- [29] T. Matsuki and T. Morii, *Phys. Rev. D* **56**, 5646 (1997); H.-Y. Shan and A. Zhang, *Chin. Phys. C* **34**, 16 (2010).